Effects of Poly(3-hexylthiophene) Molecular Weight and the Aging of Spinning Solution on the Electrospun Fiber Properties

Humayun Ahmad,[†] *Song Zhang,*[‡] *Chih-Ting Liu,*[‡] *Guorong Ma,*[‡] *Jason D. Azoulay,*[‡] *Xiaodan Gu,*[‡] *Mahesh K Gangishetty,*[¦] *Santanu Kundu*[†]*

[†]Dave C. Swalm School of Chemical Engineering, Mississippi State University, MS State, MS 39762, United States

[‡] School of Polymer Science and Engineering, University of Southern Mississippi, Hattiesburg, MS 39406, USA

[¦]Department of Chemistry & Department of Physics and Astronomy, Mississippi State University, MS State, MS 39762, United States

E-mail: santanukundu@che.msstate.edu

Keywords: Conjugated polymer, P3HT, aging, self-assembly, electrospinning, single fiber, electrical conductivity

ABSTRACT

The electrospinning technique has been considered an attractive route for processing conjugated polymers in a significant quantity for large-scale applications. The processing-structure-property relationship of the electrospinning process for conjugated polymers is not well understood. Here, we report the electrospinning of poly(3-hexylthiophene) (P3HT) for three different molecular weights of P3HT: 31, 58, and 83 kDa. Chloroform was used as a solvent, and a high molecular weight poly(ethylene oxide) (PEO) was utilized to facilitate the processing of P3HT. The electrospinning was performed on the freshly prepared and 24 h aged spinning solutions. The aging of the spinning solution led to the self-assembly of P3HT chains, particularly with dominant H-aggregation for 83 kDa P3HT. The structure development and properties of the fibers were investigated, including the single-fiber electrical conductivity measured using a custom-built setup. The electrical conductivity has been found to be increasing with increasing molecular weight, and as high as a five-fold enhancement in single fiber electrical conductivity was obtained compared to the fiber from the freshly-prepared solution. Despite a 25% PEO concentration in the fibers, the maximum electrical conductivity of a single fiber was found to be $\approx 2.7\ X\ 10^{-5}$ S/cm, similar to the pristine P3HT thin films. Our study provides an additional understanding of P3HT structure development in electrospun fibers as a function of polymer molecular weight and processing steps and relates that to fiber properties.

INTRODUCTION

Conjugated polymers (CPs) are being investigated for many applications, including in organic electronics, actuators, sensors, smart apparel, and solar cells, to name a few.[1–9] Several strategies, including developing new polymer architecture and tuning their molecular weight, controlling regioregularity, aging of the processing solution, controlled deposition methods (shear-aligning coating, slow solvent evaporation), and post-deposition treatments (thermal annealing, solvent vapor annealing) have been utilized to achieve the improvement of the charge transport properties in CPs.[6,9–17] However, most of the methods described above mostly involved thin films and were much less investigated in the context of micro- and nanofibers. Although the electrospun fibers can potentially be used in many large volume applications,[4,18–20] a fundamental understanding of the processing-structure-property relationships for the electrospinning process of CPs is still incomplete.

Among different CPs, the electrospinning of poly(3-alkylthiophene) (P3AT), especially poly(3-hexylthiophene) (P3HT), has been investigated in the past.[5,20–22] CPs generally have lower molecular weight and are less flexible because of their rigid backbone, and have limited solubility in common organic solvents.[23] As a result, CPs usually do not reach the sufficient chain entanglements in the solution required to form fibers through the electrospinning process. Different strategies have been used to aid the electrospinning process, such as adding flexible polymers, poly(ethylene oxide) (PEO) and poly(Ɛ-caprolactone), in the spinning solution of P3HT, or using a core-shell coaxial electrospinning strategy using poly(methyl methacrylate) (PMMA).[5,20,21,24,25] The usage of high molecular weight of PEO is common, which has shown to lead to uniform, bead-free fibers.[20,22,24–26] Interestingly, few studies have also reported the electrospinning of P3HT without adding any flexible polymers.[23,27–29] Although high P3HT concentration led to gelation,

electrospun fibers were still obtained.[23,28] But, the mechanism for the fiber development from the gel state was not elaborated. For commonly studied flexible polymers, the effects of viscosity and entanglement of polymer solutions on the spinning process have been widely investigated.[30] However, the rheological behavior of P3HT spinning solutions where the self-assembly of polymer chains often leads to gelation has not been well studied.

For thin films, it has been observed that the lower molecular weight of the P3HT lead to a higher crystallinity, at the expense of the tie chains between different crystallites, whereas the higher molecular weight of P3HT leads to disordered structures but better connectivity between the crystallites through long tie chains.[13,31,32] To control the intra- and intermolecular ordering of polymer chains in thin films, preaggregation or self-assembly of P3HTs chains in solution, facilitated by adding a small amount of poor solvent to the polymer solution, ultrasonication, lowering the temperature, and aging of the solution, have been investigated.[6,7,15,33,34] Previous studies have shown that the aging of the P3HT-containing solutions can lead to the formation of nanowires, and even nanowhiskers, depending upon the aging time, polymer concentration, and solvent quality.[6,33,35–37] The self-assembled CP nanostructures in solution have been shown to improve the electrical properties of the final processed films.[23,38–40] The impact of molecular weight of CPs and their self-assembly in the spinning solutions on electrospinning have not been investigated. Further, polymer chains in thin films can achieve an equilibrium structure; however, that is unlikely in electrospun fibers due to the rapid evaporation of the solvent and the high stretching force during spinning. Therefore, the properties of thin films and fibers are not directly correlated.

In the literature, the charge-transport behavior of P3HT fibers has been mostly quantified through electrical conductivity measurement of the fiber mats rather than for the single fibers.[20,24] Note

that the fiber mat conductivity values represent the bulk conductivity, appropriate for continuous film-like materials, but not for fiber mats, which have void spaces in between.[24] Therefore, conductivity measurement of the single fibers is essential to determine the processing-structure-property relationship.

Here, we report the electrospinning of P3HT by systematically varying the molecular weight and also by aging the spinning solutions that enhance the self-assembly of P3HT. We have elucidated the self-assembly process of P3HT in the solution state using spectroscopy experiments, and the gelation behavior was monitored using shear-rheometry experiments. The microstructure of fiber was further analyzed by X-ray scattering techniques. We have also determined the electrical conductivity of individual fibers using a custom-built device and linked the conductivity values to the molecular weight and aging of spinning solutions. Our work demonstrates that the P3HT molecular weight and self-assembly of P3HT chains in the spinning solution affect the electrical conductivity values of the electrospun fibers. Our results will potentially help rationally develop semiconductive polymeric fibers for smart textiles and wearable device applications.

EXPERIMENTAL SECTION

Materials

Three poly(3-hexylthiophene-2,5-diyl) (P3HT) samples were procured from Rieke Metals Inc. (Lincoln, NE) with the weight-average molecular weights of 31 kDa, 58 kDa, and 83 kDa. The polymer characteristics as provided by Rieke Metals are reported in Table S1. Note that all of these polymers had a regioregularity of 95 to 96.2 %. Based on the NMR data provided by Reike Metals, primarily HT-HT triads were found in 83 and 58 kDa, whereas, in 31 kDa it was HT-HH triads. Poly(ethylene oxide) (PEO) ($M_v \approx$ 600-1,000 kDa), chloroform (>99.5%), Fomblin Y LVAC 14/6 oil (MW ≈ 2.5 kDa) were obtained from Sigma-Aldrich. All chemicals were used as received.

Sample Preparation

Solutions of P3HT and PEO were prepared separately in individual glass vials. Particularly, 30 mg of P3HT was dissolved in 0.5 mL of chloroform, and 10 mg of PEO was added in 0.5 mL of chloroform in separate vials. Then, the vials were tightly sealed, and the solutions were stirred on a magnetic hot plate at 55 °C for two hours. P3HT and PEO solutions were then mixed at the desired ratios, and the mixture was stirred for another hour at 55 °C. In the final solution, the total concentration of P3HT and PEO was maintained at 4% (wt/v). However, four different combinations of P3HT and PEO ratios were considered, as detailed in the results and discussion section below. Table 1 displays the samples considered here, the designated sample names, and their compositions.

Table 1. Compositions of Spinning Solutions and Processed Samples (Fibers/Beads) in Solid-State

Sample name	Spinning solution composition	Fiber/bead composition	Aging
58 kDa	5 wt/v% P3HT MW 58 kDa	100 wt% P3HT MW 58 kDa	None
31 kDa_0 h	3 wt/v% P3HT MW 31 kDa + 1 wt/v% PEO MW 1000 kDa	75 wt% P3HT MW 31 kDa + 25 wt% PEO MW 1000 kDa	None
31 kDa_24 h	3 wt/v% P3HT MW 31 kDa + 1 wt/v% PEO MW 1000 kDa	75 wt% P3HT MW 31 kDa + 25 wt% PEO MW 1000 kDa	24 h
58 kDa_0 h	3 wt/v% P3HT MW 58 kDa + 1 wt/v% PEO MW 1000 kDa	75 wt% P3HT MW 58 kDa + 25 wt% PEO MW 1000 kDa	None
58 kDa_24 h	3 wt/v% P3HT MW 58 kDa + 1 wt/v% PEO MW 1000 kDa	75 wt% P3HT MW 58 kDa + 25 wt% PEO MW 1000 kDa	24 h
83 kDa_0 h	3 wt/v% P3HT MW 83 kDa + 1 wt/v% PEO MW 1000 kDa	75 wt% P3HT MW 83 kDa + 25 wt% PEO MW 1000 kDa	None

83 kDa_24 h	3 wt/v% P3HT MW 83 kDa + 1 wt/v% PEO MW 1000 kDa	75 wt% P3HT MW 83 kDa + 25 wt% PEO MW 1000 kDa	24 h

Electrospinning Process

The electrospinning was conducted using a custom-built setup shown in Figure 1. In this study, electrospinning was conducted on the spinning solutions that were freshly prepared (designated as w/o aged) and was aged for 24 h (designated as w/24 h aged). After mixing the PEO and P3HT-containing solutions in appropriate proportions, the w/o aged solution was transferred to a syringe (spinning syringe) and was electrospun immediately. For the aging process, the mixed solution was left at room temperature for about 24 h in the spinning syringe. In this case, the needle tip was dipped in chloroform to avoid the drying of chloroform leading to clogging of the tips (Figure S1).

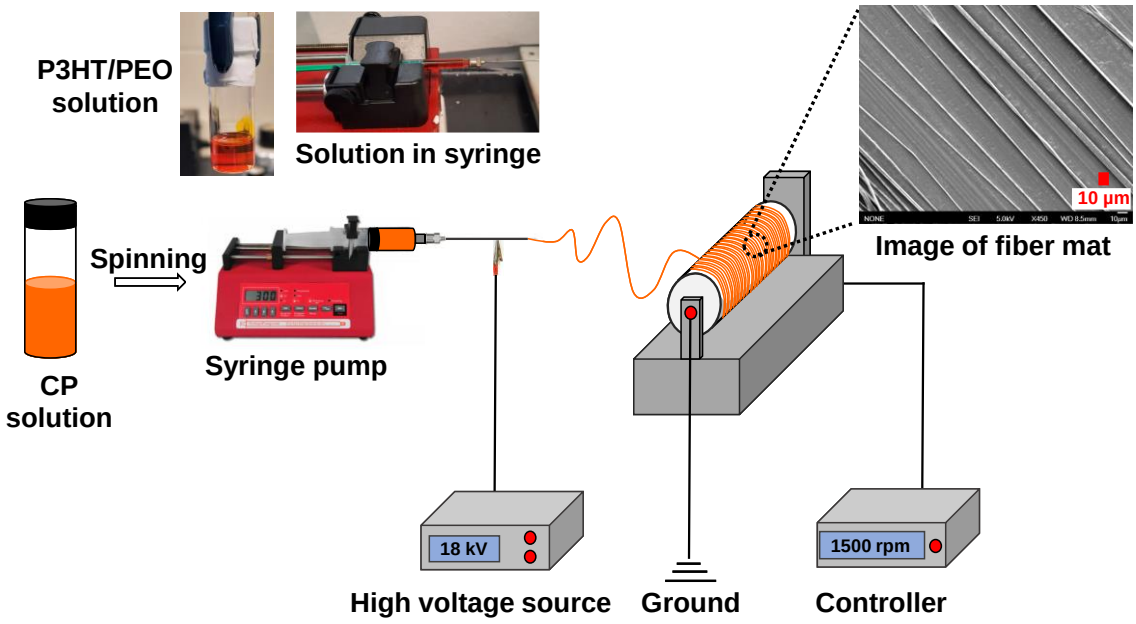

Figure 1. Electrospinning setup used for spinning P3HT fibers. Schematic showing spinning steps from solution.

A 1 mL gastight syringe with a 26-gauge flat tip metal needle was used for electrospinning. The syringe with the spinning solution was mounted on a syringe pump (NE-1000, NewEra Pump Systems Inc.). The needle was connected to a high voltage power supply (RC-5000, Tong Li Tech, China) and was placed approximately 8 cm away from a grounded rotating drum collector covered with aluminum foil for sample collections. The rotational speed of the collector was maintained at 1500 rpm for all experiments. The volumetric flow rate was maintained constant at 1.5 mL/h, and 18 kV power was used for all experiments. The needle tip was wiped and cleaned every 30-40 s to prevent the clogging of the needle tip. The experiments were conducted at room temperature (20 °C) with relative humidity ranging from 50 to 60%

Field-Emission Scanning Electron Microscope (FE-SEM)

A field-emission scanning electron microscope FE-SEM (JEOL JSM-6330F) was used at an accelerating voltage of 5 kV to image the electrospinning fibers. The electrospun fiber mat was collected on aluminum foil and was sputter-coated with an approximately 15 nm thick platinum layer to avoid charging and to enhance the quality of the micrographs. An image processing software (ImageJ) was used to measure the fiber diameters.

Rheological Study

The rheological investigations were conducted using a TA Instruments HR-2 Discovery rheometer equipped with a Peltier stage. A 25 mm parallel plate geometry was used. The samples were loaded on the bottom plate at 20 °C, and a gap of 400 μm between the upper and bottom plates was maintained. In our experimental setup, a petri dish was attached to the bottom plate, and the petri dish was filled with fluorinated oil (Fomblin Y LVAC 14/6) after the sample loading in the parallel plate geometry. The oil level was maintained slightly above the edge of the top plate. This setup (Figure S2) suppressed the chloroform evaporation during the rheological experiments.[41]

Photoluminescence Analysis

The fluorescence study of the P3HT/PEO solution was conducted using an Edinburgh FS5 Spectrofluorometer instrument. A 4 mL quartz cuvette of 1-cm path length was used to investigate solutions, whereas thin film and fiber mats were collected on 15 mm by 20 mm quartz coated glass substrates. The excitation wavelength of 450 nm was used, and the emission scans were recorded over the range of 465 to 800 nm using a slit width of 2-5 nm with a 1 nm wavelength increment and an integration time of 1 s.

Thermal Analysis

The thermal properties of electrospun fibers were analyzed using a TA instrument DSC-Q2000. DSC measurements were performed under a nitrogen atmosphere at the heating rate of 5 °C min^{-1} from -50 °C to 330 °C. Hermetically sealed aluminum pans with a sample weight varying from 2 to 5 mg were used.

X-ray Diffraction (XRD) and Grazing Incident Wide-Angle X-ray Scattering (GIWAXS)

XRD patterns were recorded in a Rigaku Ultima IV X-ray diffractometer (CuKα-radiation; λ=0.154 nm) with a scanning rate of 0.5°/min over the 2θ range of 3° to 30°. P3HT thin film and fiber mats for XRD measurements were deposited on a quartz-coated glass slide. Furthermore, the P3HT chain orientation in fiber was investigated using grazing incident wide-angle X-ray scattering (GIWAXS). A thin layer of electrospun fiber mat was collected on the Si wafer by placing it on the collector. GIWAXS measurements were conducted on XENOC Xeuss 2.0. An incident X-ray energy of 8.05 keV at an incident angle of 0.2° was used. The data was collected using the Pilatus 1M detector and analyzed in Igor 8 software using Nika package and WAXStools.

Electrical Conductivity

A custom-built multipin framework was used to measure the electrical conductivity of single electrospun fibers (Figure S3). Here, a quartz-coated glass substrate with an array of gold contacts was fabricated (chips). The gold contacts were deposited via thermal evaporation. The distance between two adjacent gold contacts varied between 30 to 80 µm. Electrospun fibers were collected on these chips. For this, electrospinning was performed for a short time, and a limited number of fibers (1-4) connecting two neighboring contacts was identified by an optical microscope image. A custom-built multipin system was used to measure the I-V responses over -2 V to 2 V using a Keithley source meter (2604B, dual-channel, 40V SMU). A minimum of three batches obtained from different spinning solutions and at least four samples from each batch, i.e., on average 12 samples were considered for each condition.

In addition, fiber mat conductivity was measured using an electrode system (IDE) from Metrohm Dropsens (Spain). The IDE has two planar interdigitated electrodes (bands/gaps: 10 µm, number of digits: 125 × 2) with two connection tracks made of platinum, fabricated on a glass substrate (L 22.8 × W 7.6 × H 0.7 mm). A thin layer of fiber mat covering the IDE's active area was collected by placing the IDE chips on the rotator. A potential was applied between the two probes using Keithley 2450 source meter. The conductivity (σ) of the fiber mat was calculated from the measured resistance (R) of the fiber mat and the cell constant of the IDE (K) using the relationship of $= \frac{K}{R}$, where K is the cell constant of the IDE chip.

RESULTS AND DISCUSSION

Electrospinning and Morphology of Electrospun Fibers

Three different molecular weights (MWs) of P3HT, 31, 58, and 83 kDa were considered here. For each molecular weight of P3HT, the spinning was performed using the freshly prepared and 24 h aged solutions. This allowed us to investigate the effects of aging on the self-assembly of P3HT in the spinning solution and the corresponding impacts on the fiber properties. The freshly prepared solution (w/o aged) at 55 °C was rapidly transferred to the syringe. The temperature dropped to room temperature at ~10 mins (Figure S4), and the spinning was conducted at room temperature. Both the aging of the spinning solution (w/24 h aged) and the subsequent spinning was conducted at room temperature without further heating of the solution.

The electrospinning of P3HT in chloroform was initially attempted considering three different P3HT (Mw: 53 kDa) concentrations: 5, 8, and 12 wt/v%. The 5 and 8 wt/v% solutions resulted in bead formation (Figure 2a-b), whereas the 12 wt/v% solution was too viscous to process, resulting in only a few beads on aluminum foil (Figure S5). Similar results have been observed for the other two molecular weights of P3HT considered here. We hypothesize that the P3HT chains rapidly formed a gel-like structure at room temperature. Although such structure likely dissociated as it flowed through the needle, there were no significant entanglements of polymer chains necessary for fiber formation for the concentration and molecular weights considered here.[24,42,43] Note that P3HT backbone rigidity results in a high entanglement molecular weight.[24]

A high molecular weight PEO (M_V~600-1000 kDa) was added to the P3HT solutions to circumvent this problem. PEO of this molecular weight has a significant chain entanglement, and it was possible to spin fibers from 1 to 4 wt/v% solutions of only PEO in chloroform (Figure S6). The PEO concentration and the P3HT to PEO ratio were varied to determine the suitable

processing window while maintaining the total polymer (P3HT + PEO) concentration of 4 wt/v%. Four different concentrations of P3HT ($M_w \approx 83$ kDa), 4%, 3.9%, 3.6%, and 3% were considered. As discussed above, 4 wt% (no PEO added) did not lead to fiber formation, whereas 3.9 and 3.6 wt% resulted in beaded fibers (Figure 2c, S7). For 3 wt/v%, smooth fibers were obtained. Therefore, the beads progressively disappeared with increasing PEO concentration in the spinning solution (Figure S7), and such observations were true even for the 24 h aged spinning solution (Figure 2d), and for all MWs of P3HT considered here (Figure 2h-j). We have considered 3 wt/v% P3HT with 1 wt/v% PEO for further detailed investigations (Table 1). For each case, we could conduct electrospinning for 30 minutes, indicating the stability of our process/system.

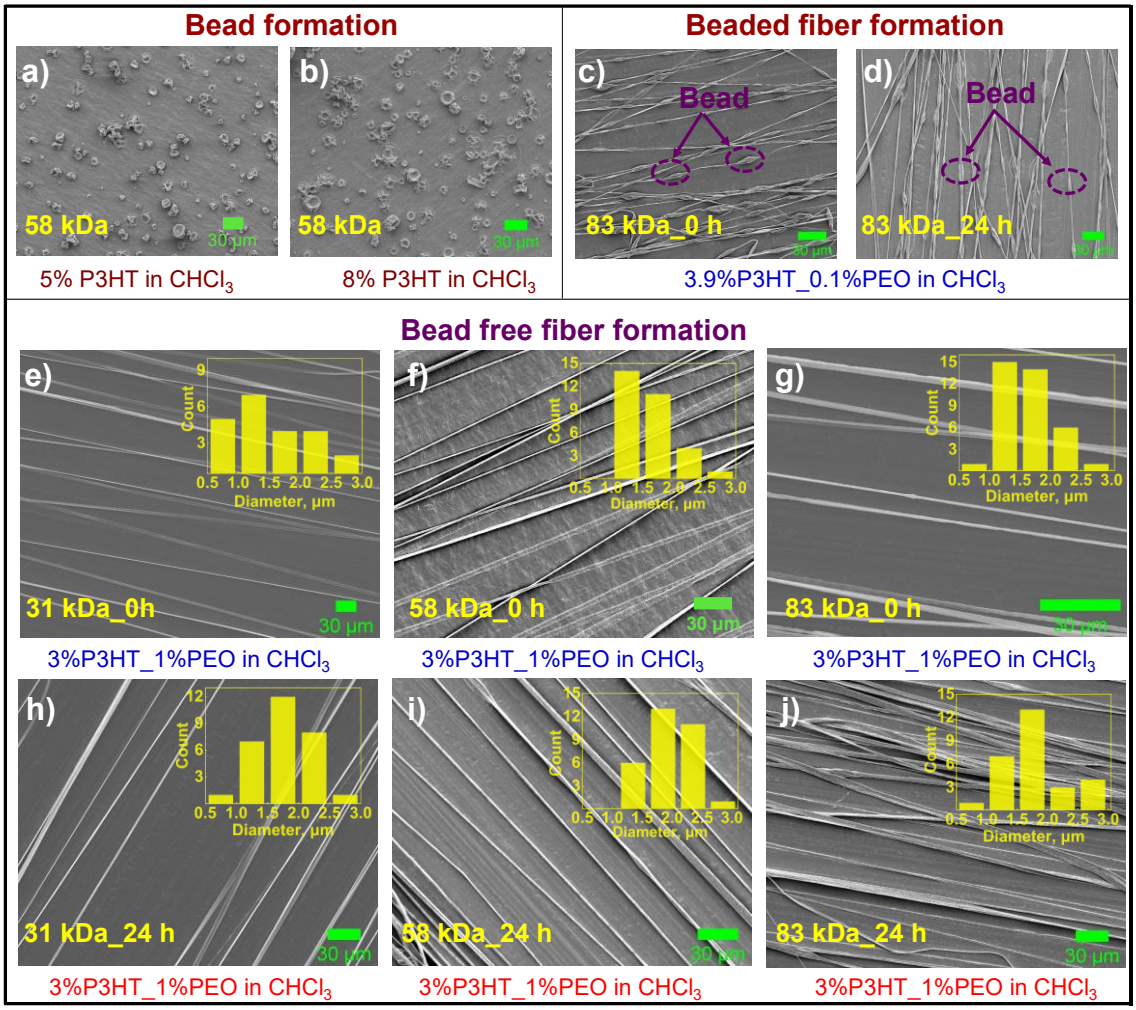

Figure 2. SEM micrographs of samples collected on aluminum foil. (a,b) Bead formation of P3HT without PEO; (c,d) Beaded fibers obtained from 3.9% P3HT (83 kDa) solution. Bead free fibers obtained from 3% P3HT solutions of different molecular P3HT weights with and without aging: (e,h) 31 kDa, (f,i) 58 kDa, and (g,j) 83 kDa. Scale bars represent 30 µm.

As observed in SEM images, the fibers were mostly cylindrical (Figure S8). The fiber diameters were measured from the SEM images, and the corresponding histograms for at least 30 individual fibers for each case are shown as insets in Figure 2e-j. These histograms indicate mostly one dominant fiber diameter. For the fibers obtained from w/o aged spinning solutions, the average fiber diameters (Figure 2e-g) were 1.80, 1.68, and 1.67 µm for 31 kDa, 58 kDa, and 83 kDa MWs

of P3HT, respectively. For w/24 h aged spinning solutions, the average fiber diameters (Figure 2h-j) were 1.70, 1.98, and 2.0 μm for 31 kDa, 58 kDa, and 83 kDa MWs of P3HT, respectively. Without aging, the fiber diameters for 58 and 83 kDa samples were similar, but 31 kDa fibers had a slightly larger diameter. With aging, a small increase in fiber diameter was observed for 58 kDa and 83 kDa. It has been shown in the literature that increasing polymer molecular weight led to the higher viscosity of the feed solutions, resulting in increased fiber diameters.[44,45] Particularly, increasing PEO molecular weight for the same polymer concentration resulted in significantly larger fiber diameter.[46] In our system, no such trend was observed, as high molecular of P3HT has led to gelation of the system. Although a small increase in fiber diameter has been noted for high molecular weight P3HT (Table S2), the t-test indicates that the difference was not statistically significant. Note that the fiber diameters reported here are larger than the typical sub-micron length scale typically reported for electrospun fibers.[20,21] We have also been able to obtain fibers with such lower diameters (Figure S9), but not considered here, as electrical conductivity measurement (as reported below) for such smaller diameter fibers was extremely challenging.

Interpreting Self-Assembly of P3HT in the Spinning Solution

The freshly prepared solutions consisting of P3HT and PEO had bright orange color, indicating their fully dissolved state. However, the solution color with 83 kDa P3HT changed from bright orange to opaque, dark red/ purple with time as it was aged in a syringe needle for 24 h (Figure S10). After 24 h of aging, the solution became gel-like. The color change and gelation indicate the self-assembly of the P3HT chains.[47,48] For 31 kDa P3HT, the solution only became slightly viscous, and the color change was insignificant, as it remained bright orange after 24 h of aging (Figure S11). The self-assembly of polymer chains in the solutions was determined by investigating their photophysical properties.

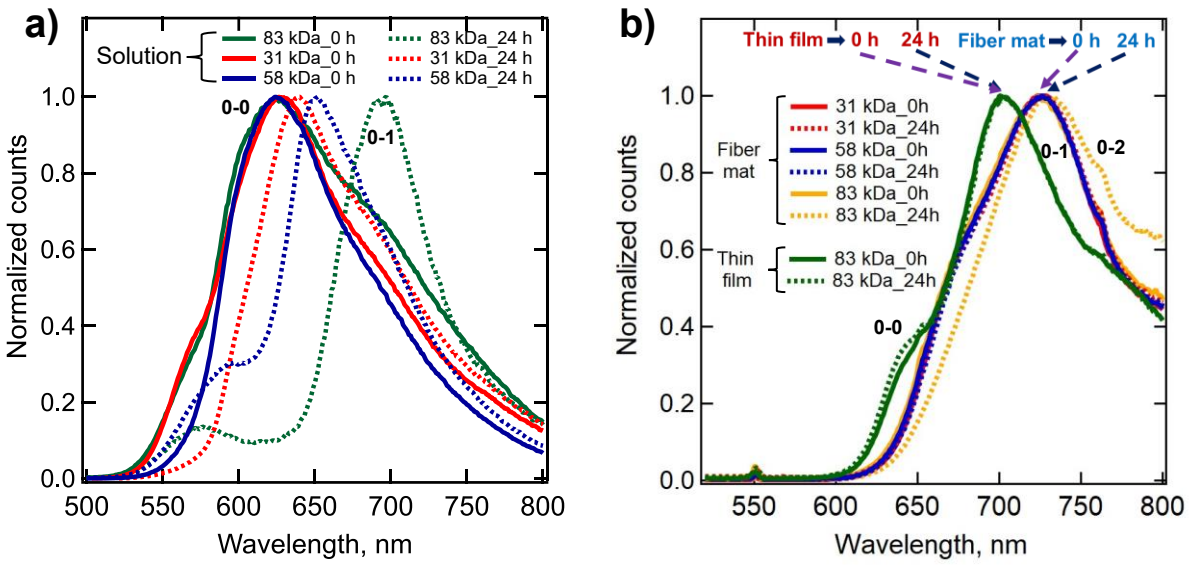

Figure 3. Photoluminescence spectra of (a) solutions of w/o and w/24 aging; b) thin film and fiber mats with different P3HT molecular weights obtained from solutions w/o and w/24 aging. The excitation wavelength was 450 nm.

Figure 3a displays photoluminescence (PL) spectra of w/o and w/24 h aged solutions with 31 kDa 58 kDa, and 83 kDa excited at 450 nm. For w/o aged solutions, one broad peak at ≈633 nm and two shoulders around 550 nm and 680 nm were observed. A clear peak around 641 nm and a shoulder around 700 nm were observed for w/24 h aged solution of 31 kDa. A broad peak between 580 to 590 nm was observed for w/24 h aged solutions of 58 kDa and 83 kDa. Further, sharp peaks at 653 nm and 697 nm were observed for 58 kDa and 83 kDa w/24 h aged solutions, respectively. The peaks at 550 and around 580 nm have been attributed to the amorphous state of P3HT, associated with the π-π* transition. [35,49] With aging, the development of the 641 nm peak for 31 kDa, 653 nm peak for 58 kDa, and 697 nm peak for 83 kDa can be attributed to the aggregation of P3HT chains,[49] confirms the self-assembly of P3HT chains during aging, even in the presence of PEO. The PL investigation of P3HT (83 kDa) without PEO was conducted (Figure S12), and it was found that PEO had assisted the self-assembly of P3HT. It has been shown earlier that self-

assembly and gelation of P3HT in solution in the presence of another component are possible, for example, for P3HT and di-Fmoc-l-lysine (a low molecular weight gelator) system in chloroform, provided P3HT and the other component are not interacting.[25,26,41] Additionally, aging the solutions for 24 hours reduced the PL intensity (counts), as shown in Figure S13. Such PL quenching was significant for the aged solutions of 58 kDa and 83 kDa, likely caused by interchain aggregation.

Next, we investigate how the self-assembly in the solution state transformed into the solid-state (fibers and films). The w/o and w/24 h aged solutions of 83 kDa P3HT were deposited as thin films on quartz plates, and the PL data of those thin films are shown in Figure 3b. For thin-film, no significant changes in peak positions occurred due to the solutions' aging. A similar trend was also observed for the other two MWs of P3HT (Figure S14)

The PL data for the fiber mats collected on the quartz slides are also shown in Figure 3b. The results for all fibers except for the fibers obtained from 24 h aged solution of 83 kDa of P3HT (83 kDa_24h) were very similar. Specifically, for all samples, except for 83 kDa_24h, a broad shoulder at 660 nm and a prominent peak at 724 nm were observed. For the 83 kDa_24h P3HT, a peak at ≈732 nm was observed, but there was no shoulder peak.

The peaks at ≈633 nm in solutions, ≈630 nm in thin films, and ≈660 nm in fibers correspond to the 0-0 vibronic transition of P3HT.[50,51] Whereas, the peaks at ≈698, 703, and 724 nm for the solutions, thin films, and the fiber mat, respectively, represent the 0-1 vibronic transition of P3HT.[50,51] Further, 0-0 and 0-1 transitions are related to the J- and H- aggregates, representing the intrachain and interchain exciton coupling, respectively.[40,50–52] The dominant aggregation type can be hypothesized based on the intensity ratio, $I_{0\text{-}0}/I_{0\text{-}1}$. [50,51,53] Except for 83 kDa_24h, $I_{0\text{-}0}/I_{0\text{-}1}>1$ was observed for all solutions, indicating significant intrachain coupling (J-aggregate) instead of

interchain one. $I_{0\text{-}0}/I_{0\text{-}1}<1$ in 83 kDa_24h solution signifies a predominantly H-aggregated system with interchain exciton coupling by promoting π−π stacking of P3HT chains. [49,50] This is also relevant to the significant solution color change due to the aging discussed above.

For both thin-film and fibers, $I_{0\text{-}0}/I_{0\text{-}1} <1$ signifies that the H-aggregation dominated over the J-aggregation. Interestingly, the PL data did not capture any detectable peak for the 0-0 band in 83 kDa_24h fibers. Thus, the H-aggregates fraction was much higher in 83 kDa_24h fibers than the fibers from both w/o and w/24h aged 31 kDa solutions. Further, in comparison to the thin film, the aggregation peaks for the fibers red-shifted as high as 31 nm (83 kDa_24h), higher than that typically reported in the literature.[26,54] The high molecular weight (83 kDa) and regioregularity (96.2%) of the P3HT sample used in this study have facilitated the self-assembly process in solution during aging. During electrospinning, the self-assembled chains may remain unchanged, and only the amorphous segments become extended because of the applied electric field, a scenario most likely the case for 83 kDa_24h. It is also possible that some of the self-assembled chains can become unfolded and extended during electrospinning. The extended P3HT chains can form π−π stacking leading to an increase of H-aggregates.[50,55] In all samples, except for 83 kDa_24h, the transformation of predominantly J-aggregates in solution to predominantly H-aggregates in fibers indicates the likely unfolding of folded chains, including J-aggregates, during electrospinning and subsequent formation of H-aggregates.[50]

Further, FTIR data (Figure S15) were used to estimate the intensity ratio of the symmetric ring stretch (I_{sym}) between 1457-1465 cm^{-1} to the asymmetric (I_{asym}) ring stretch between 1510- 1512 cm^{-1}.[56] The I_{sym}/I_{asym} ratio can be utilized to understand the effect of molecular weight and aging on the conjugation length of the P3HT. High molecular weight P3HT (83 kDa) fibers from 24 h aged solution displayed the lowest I_{sym}/I_{asym} ratio (Table S5), indicating a high conjugation length

for that sample.[57,56] Such an increase in conjugation length can be attributed to the increased interchain association, as discussed above. Note that we have observed a maximum ±4 nm peak shift between experiments because of small fluctuations of P3HT and PEO weight ratios and slight variation in the sample preparation conditions (hot plate temperature, relative humidity), however, the overall trend remained the same.

Rheological Response of Spinning Solutions

As the self-assembly of P3HT in the solution can lead to changes in rheological responses affecting the spinning behavior, we conducted shear-rheometry at room temperature on the w/o and w/24h aged solutions of 31 kDa and 83 kDa P3HT using the custom-built setup shown in Figure S2.

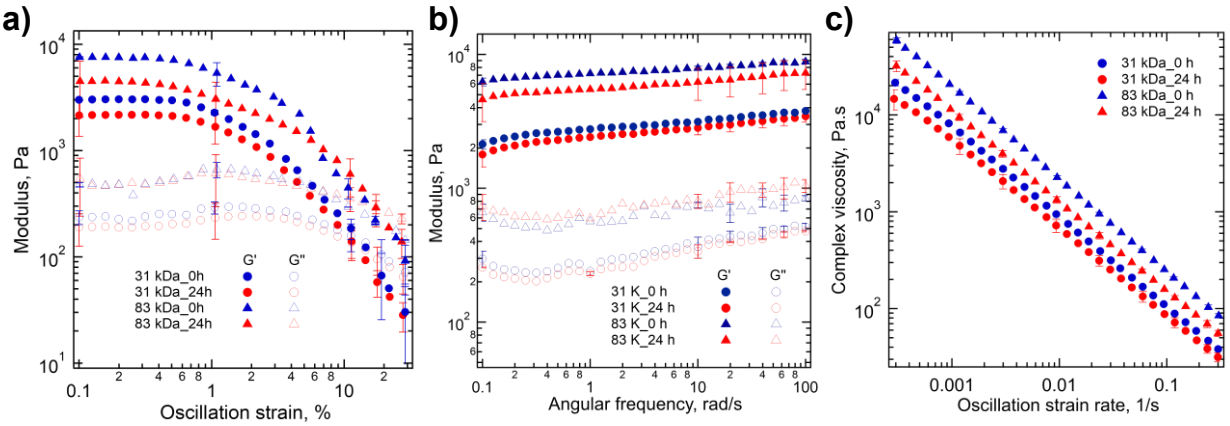

Figure 4. a) Storage (G′) and loss (G″) moduli as a function of oscillation strain amplitude captured at the frequency (ω) of 1 rad/s, b) G′ and G″ as a function of frequency, and c) complex viscosity vs. oscillation strain rate. All experiments carried out at room temperature of 20 °C. Representative error bars are shown.

Figure 4a displays the storage (G′) and loss (G″) moduli as a function of oscillation strain amplitude (γ_0) for the solutions of 31 kDa and 83 kDa P3HT. For $\gamma_0 < 0.5\%$, G′ was higher than G″ and was independent of γ_0, indicating soft-solid or gel-like behavior.[58–62] However, for $\gamma_0 >$

0.5%, G′ decreased with applied strain. In addition, G″ slightly increased for $\gamma_0 > 0.6\%$ and then decreased for $\gamma_0 > 1\%$. A crossover of G′ and G″ was observed at a higher γ_0 value. These results signify that the underlying structure was disrupted at higher strain amplitude, and the sample became more fluid-like. For both molecular weights, a decrease of G′ and G″ was observed with aging; particularly, a significant drop in G′ for 83 kDa_24h P3HT has been observed. At this stage, the origin of such a decrease with aging is unknown and will be further investigated in a future study.

Figure 4b displays G′ and G″ as a function of angular frequency for the samples w/o and w/24 h of aging. Frequency sweep experiments were performed over the frequency range of 0.1–100 rad/s using an oscillation strain amplitude of 0.3%, which was within the LVE region. Both G′ and G″ displayed weak frequency dependency, further capturing the soft solid-like behavior of these samplers at low strain amplitude, as observed in the amplitude sweep experiments.

The gelation of the P3HT and PEO in chloroform has not been reported in the literature. However, the gelation behavior of pure P3HT solution at high concentrations and a system consisting of low concentrations of P3HT and a low molecular weight gelator have been reported earlier. [41,63–66] In those gels, the P3HT chains have been shown to self-assemble to form nanofibers. Besides, those gel systems have moduli similar to that presented here.[64–66]

The estimated complex viscosity values as a function of the oscillation strain rate are shown in Figure 4c. It was difficult to obtain shear-viscosity data at high shear rates for our samples (steady shear viscosity over a limited shear rate range is presented in Figure S16); therefore, we are considering complex viscosity as a function of oscillation strain rate as the representative shear-rate dependent response. Although the applicability of the Cox-Mertz rule for this system was not

verified here, the complex viscosity values can provide some additional insights. The complex viscosity decreased with increasing oscillation strain rate for both samples.

The shear and extensional viscosity values have been shown to affect the spinnability of a polymer solution,[67] however, the spinnability of a gel-like system is not well understood. We estimated the wall shear rate for the volumetric flow rate (Q) considered here as $\dot{\gamma}_w = \frac{4Q}{\pi R_N^3} \sim 250\ s^{-1}$. Here, R_N the internal radius of the needle. By considering the shear-thinning behavior observed in Figure 4c, the viscosity values at these shear/strain rates were low, and it was possible to electrospun the solutions. We hypothesize that the weak gel-like sample dissociated into a viscous solution because of the shear stress as it flowed through the needle. Note that the shear viscosity did not decrease monotonically with $\dot{\gamma}$ and the response was slightly different from the complex viscosity, but the underlying mechanism was not investigated as it was beyond the scope of this manuscript.

Thermal Behavior of Fiber Mats

Both P3HT and PEO are semicrystalline polymers, and it is expected that these polymers form crystalline domains within the fibers. We used a differential scanning calorimeter (DSC) and x-ray diffraction (XRD) to investigate these. The measured melting temperatures of bulk P3HT used here were ≈240.8 (31 kDa), 244.8 (58 kDa), 247.1 °C (83 kDa), and that for PEO powder and PEO fibers were 67.5, and 59.5 °C, respectively (see Figure S17 and Figure S18 for the thermograms), values similar to that reported in the literature.[21,68]

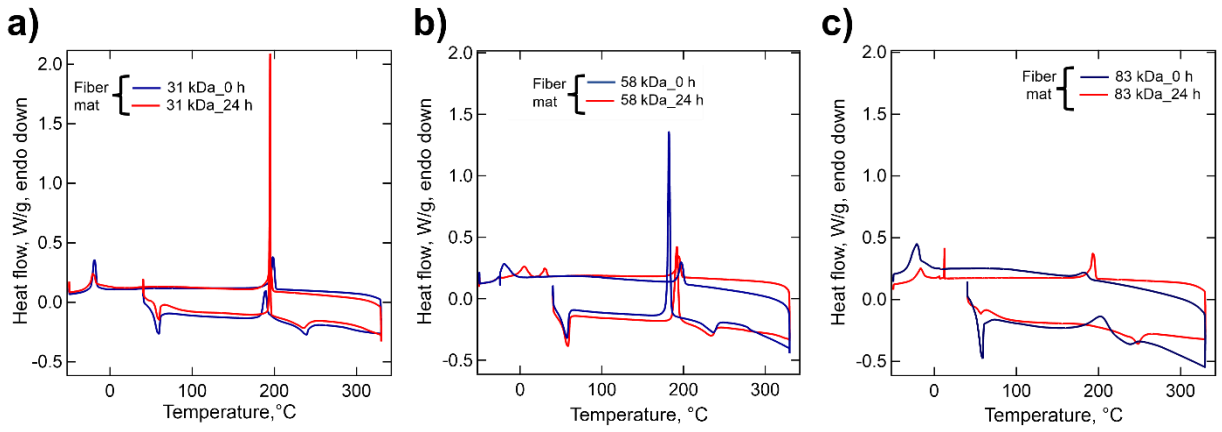

Figure 5. Differential scanning calorimetry results (first heating and cooling scan) for the electrospun fibers: a) 31 kDa P3HT, b) 58 kDa P3HT, and c) 83 kDa P3HT

Figure 5a displays DSC thermograms for 31 kDa_0h and 31 kDa_24h fibers. For 31 kDa_0h fibers, two endothermic peaks at ~59.5 and 238 °C in the first heating cycle capture the melting of PEO and P3HT, respectively. For the 31 kDa_24h fibers, PEO and P3HT melting temperature did not change significantly in comparison to 31 kDa_0h fibers. These were also in the same range as obtained for pristine P3HT and PEO samples. In addition, a sharp exothermic peak at 195 °C was observed for the 31 kDa_24 h fibers, however, the peak was less sharp (at ≈ 190 °C) for the 31 kDa_0 h fibers. This exothermic peak was likely due to the recrystallization of P3HT. For PEO fibers without P3HT such a peak was not observed. As expected, in the second heating cycle, the recrystallization peak was not observed (Figure S19). The exothermic peaks in the cooling cycle captured the crystallization of P3HT and PEO components. For 58 kDa, the melting temperature of P3HT and PEO did not change significantly with the aging of the spinning solutions (Figure 5b). Note that the exothermic peak for 58 kDa_24h fibers was less intense than 31 kDa_24h.

For 83 kDa_0h fibers (Figure 5c), similar to the 31 kDa fibers, melting peaks at ~60 °C (PEO) and ~240 °C (P3HT) were observed. In 83 kDa_24h fibers, the PEO melting peaks remained similar, but the P3HT melting peak shifted from 240.2 °C to 248.5 °C, indicating the presence of a more

ordered (crystalline) structure in that sample.[21] For 83 kDa_0h fibers, a recrystallization peak at 205.5 °C was observed, however, such a clear peak was not observed for 83 kDa_24h fibers. The recrystallization peaks indicate that the highly volatile chloroform rapidly evaporated from the electrospun fibers, suppressing the crystallization of P3HT. Those kinetically frozen chains started to recrystallize in the first heating cycle.[21,69] For the 83 kDa_24 h fibers, the chains were already highly self-assembled, and during heating in DSC experiments, further crystallization did not take place. Thus, an increase in overall crystallinity is expected in this sample.

Microstructure of the Fibers

The microstructure of the pristine P3HT, PEO powders, drop-casted pure P3HT and P3HT/PEO thin films, fiber mats for different molecular weights of P3HT, and aging conditions have been investigated using XRD. Figure 6a displays the normalized XRD spectra (data without normalization are shown in Figure S20a) collected for pristine P3HT thin film (58 kDa), P3HT/PEO thin films (P3HT 83 kDa) from w/o and w/24 h aged solutions. For thin films, the solutions were drop-casted on a quartz-coated glass substrate and were slowly dried to facilitate the self-assembly of P3HT chains. The scattering profiles were normalized based on the (100) peak intensity of P3HT and were also background corrected (typical profiles without background correction are shown in Figure S20).

The pristine P3HT thin-film displayed characteristic peaks at $2\theta \approx 5.3°$, 10.8°, and 16.3° related to the (100), (200), and (300) planes, respectively. For pristine PEO thin film, the peaks at $2\theta \approx 19.1°$ and 23.3° (Figure S21) are for the (120) and (112) planes, respectively.[69] The P3HT/PEO thin film from w/o and w/24 h aged solutions displayed the presence of all characteristic peaks of P3HT and PEO. However, the peak at ~23° was sharper for the 83 kDa_24 h. This could be an overlap of the (010) peak of P3HT and (112) peak of PEO. The (010) peak corresponds to the interchain π-π

stacking of P3HT.[21,70] The strong (100) P3HT peak indicates lamellar stacking in P3HT, both with and without PEO.[20,21]

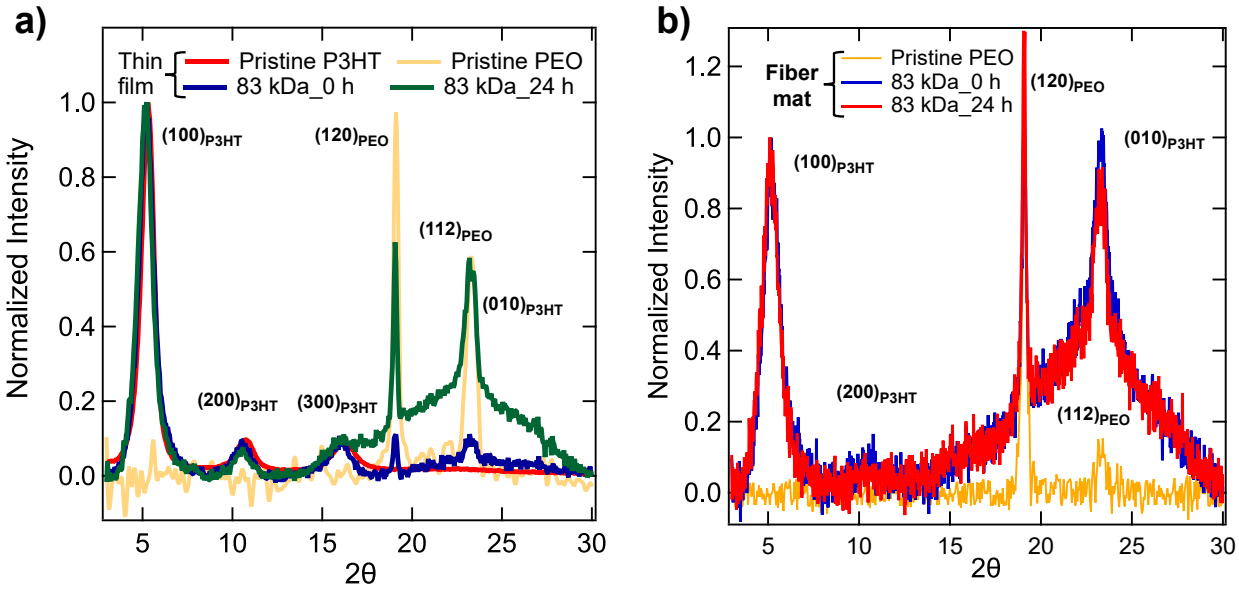

Figure 6. X-ray diffraction patterns for: a) thin films of pristine P3HT (58 kDa), PEO, and P3HT (83 kDa) with PEO; b) electrospun P3HT (83 kDa) with PEO, and PEO fiber mats. The (100) peak intensity of P3HT was considered for the normalization of XRD data.

For the fibers shown in Figure 6b (data without normalization and background correction are shown in Figure S20b), peaks at 2θ = 5.2°, 19.1°, and 23.2° represent the diffraction peaks from (100) planes of P3HT, (120) planes of PEO, and (010) planes of P3HT, respectively. The 23.2° peak was more pronounced than that observed for the thin film. Thus, both lamellar and π-π stacking of P3HT chains were present in the fibers. Similar behavior was observed for the other two molecular weight P3HT fiber mats at both aging conditions (Figure S22). For pristine PEO fibers, only (120) peak was observed (Figure S21). The absence of (112) peak has been attributed to the small fiber diameter that most likely restricted the size of (112) planes, resulting in a

reduction of peak intensity or elimination of the peak.[68,71] Note that the (120) PEO peak in Figure 6b is greater than unity, as the intensity of this peak is higher than that of (100) peak of P3HT. The full-width half maxima (FWHM) values for different peaks have been estimated (Table S6). For the 83 kDa_24h fibers, the FWHM values for both lamella and π-π stacking directions were lower than those observed in the 83 kDa_0h fibers. The reductions of FWHM further indicate that 83 kDa_24h P3HT fibers were more crystalline, consistent with the DSC results.

Any possible orientation of crystalline domains in the fibers was investigated by capturing GIWAXS data on the fiber mats. The 2D and 1D scattering profiles for all three P3HT molecular weight fiber mats from w/o and w/24 h aged spinning solutions are shown in Figure S23 and Figure S24, and the results for 83 kDa_24 h fiber mat are presented in Figure 7. We considered two cases where the incident beam was either perpendicular or parallel to the long-axis direction of fibers (Figure 7a-b). The out-of-plane and in-plane 1D intensity vs. scattering vector plots are shown in Figure 7c-d.

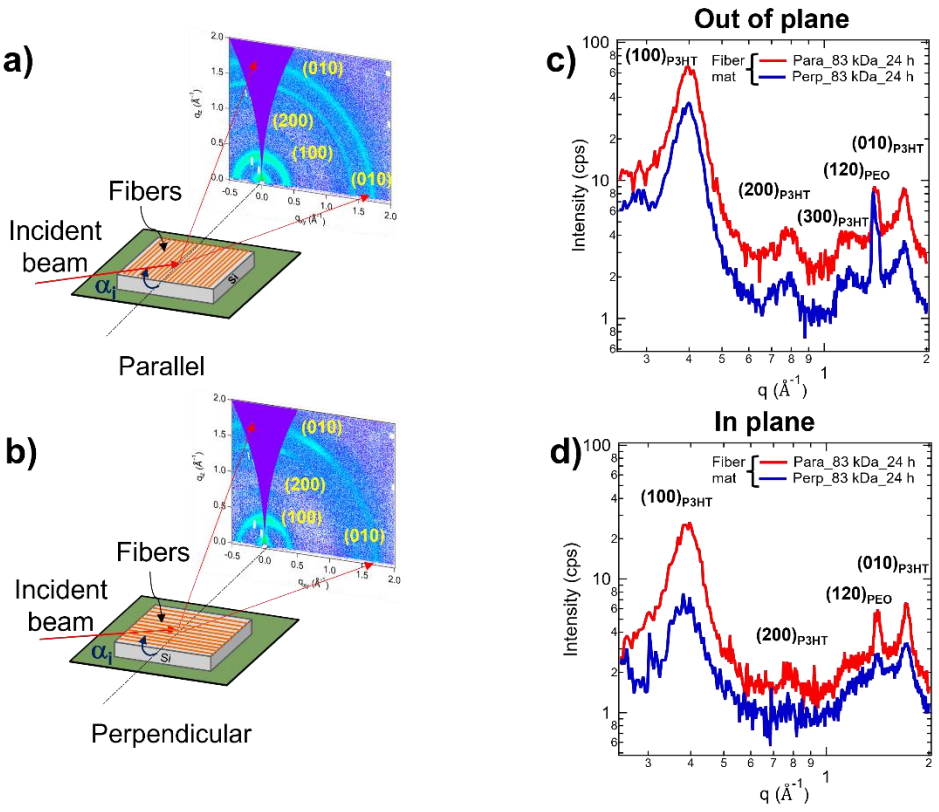

Figure 7. 2D GIWAXS patterns of fiber mat for 83 kDa_24 h aligned a) parallel, b) perpendicular to the incident beam direction. 1D GIWAXS profiles for (c) out-of-plane and (d) in-plane directions. "Para" and "Perp" in figure legends represent incident beam parallel and perpendicular to the fiber long-axis, respectively.

In Figure 7c-d, several strong peaks in the low q region, from q ≈ 0.4 to 1.2 Å^{-1}, both in- and out-of-plane directions, can be observed. These peaks correspond to the well-ordered lamellar stacking of alkyl chains.[20,21,72] For the incident beam perpendicular to the fiber axis, strong higher order reflections of (100) alkyl stacking peak, i.e., second order (200) peak at q ≈ 0.8 Å^{-1}, and third order (300) peak at q ≈1.2 Å^{-1} were observed in the out-of-the plane profile, but the higher order peaks were not very evident in the in-plane direction. Higher order reflections indicate a more perfect crystallite structure.[72] In addition, the presence of higher-order reflections in out-of-plane can be attributed to the edge-on orientation with respect to the fiber axis.

In the high q region from 1.2 to 1.8 $Å^{-1}$, strong peaks at $q \approx 1.4$ $Å^{-1}$ and at $q \approx 1.7$ $Å^{-1}$ were also observed. These correspond to the (120) peak of PEO, and (010) peak of P3HT, respectively. The presence (010) peak suggests the existence of π-π stacking, and the intensity of this peak was higher in the out-of-plane direction than in the in-plane direction. This signifies a face-on orientation with respect to the fiber axis. Thus, we can conclude that this sample has a mixed P3HT orientation, including edge-on and face-on structures with respect to the fiber axis.

Further, as presented in Figures S23 and S24, for the cases of incident beam perpendicular to the fiber direction, higher order reflections of (100), and (010) peak with high intensity were observed. This indicates a mixed orientation of P3HT in all fibers irrespective of their molecular weight and aging conditions. Note that the higher rotational speed of the collector can have an impact on the orientation development and needs to be investigated further.

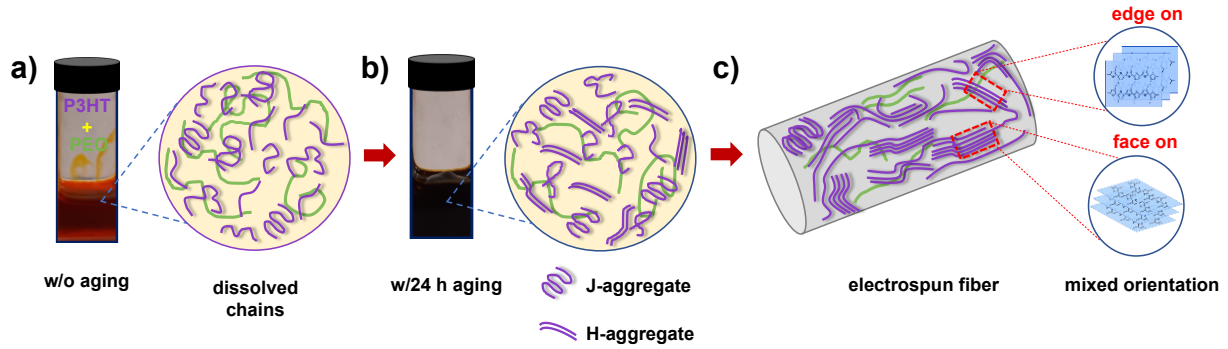

Figure 8. Schematic representation of microstructure evolution of P3HT in solution and then to fibers. (a) The freshly prepared solution; b) Evolution of H- and J- aggregates during aging of the solution; c) Presence of both face-on and edge-on oriented P3HT structures in a fiber. Here, PEO chains are in green, and P3HT chains are in purple.

Based on all characterization data presented above, the microstructure development from the fresh solution to the aged solution and then to fibers is shown in Figure 8. With aging, the self-assembly of P3HT chains leads to the formation of J- and H-aggregates. However, the predominance of one type of aggregates in comparison to the other depends on the P3HT molecular weight. During electrospinning, the amorphous chain can become extended, and the self-assembled structure may remain unchanged. Alternatively, some folded polymer chains can unfold and be extended because of the applied electric field. The extended chains can form H-aggregates, becoming a predominant structure in the electrospun fibers. In the fibers, a mixture of face-on and edge-on structures has been found. Longer chains for high molecular weight fibers can act as tie chains between the ordered regions.

Electrical Conductivity of the Fibers

We studied the room temperature electrical conductivity of the single electrospun fiber using a custom-built setup and for fiber mats using IDE chips. The fiber mat conductivity values were found to be ~10^{-7} S/cm, two orders of magnitude higher than that reported in the literature.[20,24]

Note that the IDE chips provide the bulk conductivity values which is appropriate for thin films but not for the discontinuous and poorly aligned electrospun fibers as found in fiber mats (see Figure S25). Although most commonly reported in the literature, the bulk conductivity values are not highly beneficial. Instead, the single fiber conductivity values can be directly related to the polymer properties and processing conditions. Here, we aimed to measure the conductivity of single fiber using a specially designed chip shown in Figure S3a. We targeted to collect a single fiber connecting the two gold contacts on a chip, but because of the experimental challenges, we often collected multiple fibers, as high as four fibers (Figure S3d).

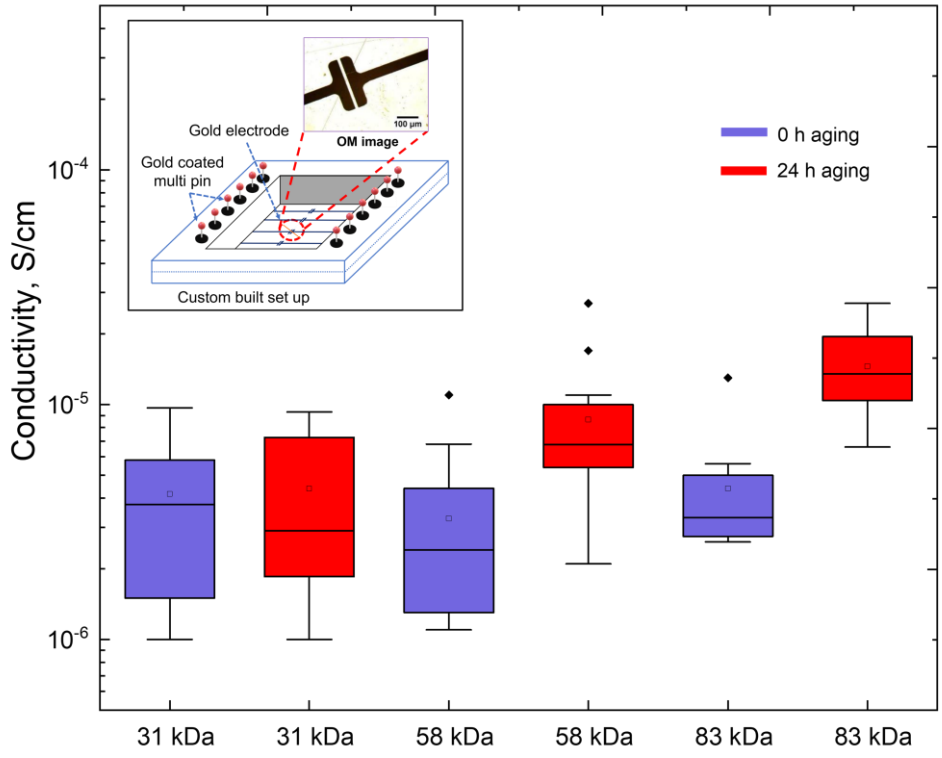

Figure 9. Electrical conductivity of P3HT/PEO single fibers as a function of the P3HT molecular weight and aging conditions of the spinning solution. For each condition minimum of 12 sets of samples were characterized.

For our system, the linear current-voltage (I–V) curves confirmed the ohmic behavior of these samples.[23,73] For a single fiber connecting the gold contacts, electrical conductivity (σ) was obtained by using the following equation (1),

Single fiber conductivity, $\sigma = \frac{1}{\rho} = \frac{I}{V} * \frac{L}{A} = \frac{\frac{I}{V}}{\pi(\frac{R^2}{L})}$ (1)

Where A, I, V, L, and R are the fiber cross-sectional area, current, voltage, length, and radius of fiber, respectively. As discussed above, all fibers were considered cylindrical (Figure S8). However, if we have more than one fiber connecting the gold contacts, the equation (1) can be modified as below to estimate the single fiber conductivity,

$$\sigma = \frac{1}{\rho} = \frac{\frac{I}{V}}{\pi \sum_{i=1}^{n} \frac{R_i^2}{L_i}} \quad (2)$$

Where L_i and R_i are the length and radius of the i^{th} fiber captured from optical micrographs. I and V are the overall current and applied voltage.

Figure 9 shows the σ for all three molecular weights of P3HT and at the two aging conditions. The molecular weight of P3HT plays a role in σ, particularly for the higher molecular weight, as σ for 83 kDa fibers has been found to be statistically higher than 58 kDa. The aging of the spinning solution played a role on σ for 58 and 83 kDa fibers, but not for 31 kDa fibers. σ increased by two times from 58 kDa_0h to 58 kDa_24h fiber. For 83 kDa, the change was more significant. The maximum conductivity of 2.75×10^{-5} S/cm was obtained for the 83 kDa_24h fibers, which was about five times higher than 83 kDa_0h.

A significant enhancement of electrical conductivity for 83 kDa_24h fibers can be attributed to two factors. First, as indicated above, the long polymer chains in the high molecular weight of P3HT may act as a tie chain between the ordered regions, facilitating charge transport and

increasing electrical conductivity.[74] Second, the conjugation length was higher for 83 kDa_24 h because of interchain aggregation, which likely resulted in a further increase in conductivity through the interchain hopping mechanism.[75] Hence, high molecular P3HT fibers obtained from the aged solutions have more ordered P3HT crystallites and an interconnected and percolated structure with higher electrical conductivity. In comparison, these two characteristics were lesser for the low molecular weight fibers, likely resulting in lower conductivities.

The σ values of blade-coated thin films of pristine 83 kDa P3HT from w/o and w/24h aged solutions are reported in Table S6 for comparison. The electrical conductivities of the fibers were found to be similar to the pristine 83 kDa P3HT thin films measured here (Table S6), and that reported in the literature.[76] Note that the electrospun fibers considered here contained 25% PEO, an insulating material. In addition to PEO, other flexible polymers will be considered in future research, and other types of conjugated polymers will also be considered.

CONCLUSIONS

In this study, we have successfully processed P3HT/PEO into fibers using the electrospinning technique. We have captured the self-assembly behavior of P3HT in the spinning solution in the presence of PEO. The P3HT/PEO solutions displayed color change during the 24 h aging process, indicating time-dependent polymer aggregation. Correspondingly, the PL data demonstrated that the significant self-assembly/aggregation of P3HT chains occurred for 83 kDa P3HT, the highest molecular weight considered here. The PL data also captured the transformation from J- to H-aggregates in solution facilitated by the high molecular weight P3HT and 24 h aging, indicating the interchain exciton coupling by promoting π–π stacking of P3HT chains. The preexisting H-aggregates in the solution were retained and even increased during the processing of electrospun

fibers. The shear-rheometry indicates that the self-assembly of the high molecular weight P3HT chains within the solution led to gelation. We hypothesized that the shear stress in the needle during processing dissociated the gel structure and facilitated the spinning. The GIWAXS analysis for the samples investigated here suggested that polymer crystals were randomly oriented with respect to the fiber axis. This study captured the effect of P3HT molecular weight, PEO concentration, and the aging of the spinning solution on the electrical conductivities. The electrical conductivity of fibers increased with the molecular weight and aging of the solution. As high as five-fold enhancement in single fiber electrical conductivity was obtained for the aged high molecular weight P3HT solution compared to the fibers from without an aged solution.

ASSOCIATED CONTENT

Supporting Information. A table presenting P3HT grades used here; diameters of all fibers; thermal properties of all molecular weights fiber mats; photophysical properties; $I_{sym}/I_{asym\ values}$; XRD data for P3HT/PEO fiber mats; thin-film and single fiber conductivities; an image of the experimental setup for P3HT aging in the needle; schematic of rheology setup; gold patterned custom-built setup for single fiber conductivity measurement; temperature profile of spinning solution; SEM micrograph of beads from 12 wt/v% P3HT; OM images of PEO electrospun fibers; progressive transformation of beads to fibers; SEM images of cylindrical fiber; SEM image of sub-micron fibers; color change of P3HT/PEO in chloroform at room temperature due to aging for 83 kDa, and 31 kDa; PL data capturing effect of PEO on aging; PL quenching behavior of P3HT and PEO solution; PL spectra of thin films; FTIR study of thin film and fiber mat; steady shear viscosity as a function of shear rate; DSC thermograms of pristine P3HT, PEO powders and fiber

mats; DSC thermogram of PEO fiber mat; DSC thermogram of fiber mat including second heating and cooling cycle; XRD raw data for drop-casted thin film and electrospun fiber mat; background corrected XRD data for PEO thin film and fiber mat; background corrected XRD data for all molecular weights of P3HT; 2D GIWAXS analysis for all fiber mats; 1D GIWAXS profiles for all fiber mats; IDE chips with fiber mat and thin-film; single fiber and fiber conductivity measurement details.

AUTHOR INFORMATION

Corresponding Author

Santanu Kundu, santanukundu@che.msstate.edu

Author Contributions

HA and SK designed the experiments and conducted the data analysis and interpretation. HA conducted the experiments. SK conceptualized and oversaw the research. The manuscript was written by HA and SK and included feedback from all authors. SZ, GM and XG performed the GIWAXS experiments and analyzed the data; MG assisted in designing a custom-built device holder for single fiber conductivity measurements; CL and JA provided the Au patterned electrode chips and carried out the initial single fiber conductivity measurements. All authors have approved the final version of the manuscript.

Funding sources

This material is based on work supported by the National Science Foundation under Grant No. 1757220.

Notes

The authors declare no competing financial interest.

ACKNOWLEDGMENT

The authors acknowledge Dr. Lifeng Huang for assisting in the preliminary single fiber conductivity measurement.

REFERENCES

(1) Kuo, C. C.; Wang, C. T.; Chen, W. C. Poly(3-Hexylthiophene)/Poly(Methyl Methacrylate) Core-Shell Electrospun Fibers for Sensory Applications. *Macromol. Symp.* **2009**, *279* (1), 41–47. https://doi.org/10.1002/masy.200950506.

(2) Nanofibers, P.; Lee, S. W.; Lee, H. J.; Choi, J. H.; Koh, W. G.; Myoung, J. M.; Hur, J. H.; Park, J. J.; Cho, J. H.; Jeong, U. Periodic Array of Polyelectrolyte-Gated Organic Transistors from Electrospun. **2010**, *Nano Lett.* 347–351. https://doi.org/10.1021/nl903722z.

(3) Sundarrajan, S.; Murugan, R.; Nair, A. S.; Ramakrishna, S. Fabrication of P3HT/PCBM Solar Cloth by Electrospinning Technique. *Mater. Lett.* **2010**, *64* (21), 2369–2372. https://doi.org/10.1016/j.matlet.2010.07.054.

(4) Chen, J. Y.; Wu, H. C.; Chiu, Y. C.; Lin, C. J.; Tung, S. H.; Chen, W. C. Electrospun Poly(3-Hexylthiophene) Nanofibers with Highly Extended and Oriented Chains through Secondary Electric Field for High-Performance Field-Effect Transistors. *Adv. Electron. Mater.* **2015**, *1* (1–2), 3–6. https://doi.org/10.1002/aelm.201400028.

(5) Chen, J. Y.; Kuo, C. C.; Lai, C. S.; Chen, W. C.; Chen, H. L. Manipulation on the Morphology and Electrical Properties of Aligned Electrospun Nanofibers of Poly(3-Hexylthiophene) for Field-Effect Transistor Applications. *Macromolecules* **2011**, *44* (8), 2883–2892. https://doi.org/10.1021/ma102286m.

(6) Kleinhenz, N.; Rosu, C.; Chatterjee, S.; Chang, M.; Nayani, K.; Xue, Z.; Kim, E.; Middlebrooks, J.; Russo, P. S.; Park, J. O.; et al. Liquid Crystalline Poly(3-Hexylthiophene)

Solutions Revisited: Role of Time-Dependent Self-Assembly. *Chem. Mater.* **2015**, *27* (7), 2687–2694. https://doi.org/10.1021/acs.chemmater.5b00635.

(7) Persson, N. E.; Chu, P. H.; McBride, M.; Grover, M.; Reichmanis, E. Nucleation, Growth, and Alignment of Poly(3-Hexylthiophene) Nanofibers for High-Performance OFETs. *Acc. Chem. Res.* **2017**, *50* (4), 932–942. https://doi.org/10.1021/acs.accounts.6b00639.

(8) Park, B.; Aiyar, A.; Park, M. S.; Srinivasarao, M.; Reichmanis, E. Conducting Channel Formation in Poly(3-Hexylthiophene) Field Effect Transistors: Bulk to Interface. *J. Phys. Chem. C* **2011**, *115* (23), 11719–11726. https://doi.org/10.1021/jp111677x.

(9) Aiyar, A. R.; Hong, J. Il; Reichmanis, E. Regioregularity and Intrachain Ordering: Impact on the Nanostructure and Charge Transport in Two-Dimensional Assemblies of Poly(3-Hexylthiophene). *Chem. Mater.* **2012**, *24* (15), 2845–2853. https://doi.org/10.1021/cm202700k.

(10) Liu, J.; Mikhaylov, I. A.; Zou, J.; Osaka, I.; Masunov, A. E.; McCullough, R. D.; Zhai, L. Insight into How Molecular Structures of Thiophene-Based Conjugated Polymers Affect Crystallization Behaviors. *Polymer (Guildf).* **2011**, *52* (10), 2302–2309. https://doi.org/10.1016/j.polymer.2011.03.026.

(11) Zhai, L.; Khondaker, S. I.; Thomas, J.; Shen, C.; Mcinnis, M. Ordered Conjugated Polymer Nano- and Microstructures : Structure Control For. *Nano Today* **2015**, *9* (6), 705–721. https://doi.org/10.1016/j.nantod.2014.10.004.

(12) Giri, G.; Delongchamp, D. M.; Reinspach, J.; Fischer, D. A.; Richter, L. J.; Xu, J.; Benight, S.; Ayzner, A.; He, M.; Fang, L.; et al. Effect of Solution Shearing Method on Packing and

Disorder of Organic Semiconductor Polymers. *Chem. Mater.* **2015**, *27* (7), 2350–2359. https://doi.org/10.1021/cm503780u.

(13) Koch, F. P. V.; Rivnay, J.; Foster, S.; Müller, C.; Downing, J. M.; Buchaca-Domingo, E.; Westacott, P.; Yu, L.; Yuan, M.; Baklar, M.; et al. The Impact of Molecular Weight on Microstructure and Charge Transport in Semicrystalline Polymer Semiconductors-Poly(3-Hexylthiophene), a Model Study. *Prog. Polym. Sci.* **2013**, *38* (12), 1978–1989. https://doi.org/10.1016/j.progpolymsci.2013.07.009.

(14) Brinkmann, M.; Rannou, P. Molecular Weight Dependence of Chain Packing and Semicrystalline Structure in Oriented Films of Regioregular Poly(3-Hexylthiophene)Revealed by High-Resolution Transmission Electron Microscopy. *Macromolecules* **2009**, *42* (4), 1125–1130. https://doi.org/10.1021/ma8023415.

(15) Mauer, R.; Kastler, M.; Laquai, F. The Impact of Polymer Regioregularity on Charge Transport and Efficiency of P3HT:PCBM Photovoltaic Devices. *Adv. Funct. Mater.* **2010**, *20* (13), 2085–2092. https://doi.org/10.1002/adfm.201000320.

(16) Chang, M.; Lim, G. T.; Park, B.; Reichmanis, E. Control of Molecular Ordering, Alignment, and Charge Transport in Solution-Processed Conjugated Polymer Thin Films. *Polymers (Basel).* **2017**, *9* (6), 23–31. https://doi.org/10.3390/polym9060212.

(17) Park, M. S.; Aiyar, A.; Park, J. O.; Reichmanis, E.; Srinivasarao, M. Solvent Evaporation Induced Liquid Crystalline Phase in Poly(3-Hexylthiophene). *J. Am. Chem. Soc.* **2011**, *133* (19), 7244–7247. https://doi.org/10.1021/ja110060m.

(18) Chen, J. Y.; Hsieh, H. C.; Chiu, Y. C.; Lee, W. Y.; Hung, C. C.; Chueh, C. C.; Chen, W. C. Electrospinning-Induced Elastomeric Properties of Conjugated Polymers for Extremely Stretchable Nanofibers and Rubbery Optoelectronics. *J. Mater. Chem. C* **2020**, *8* (3), 873–882. https://doi.org/10.1039/c9tc05075b.

(19) Serrano-Garcia, W.; Bonadies, I.; Thomas, S.; Guarino, V. P3HT Loaded Piezoelectric Electrospun Fibers for Tunable Molecular Adsorption. *Mater. Lett.* **2020**, *266*, 127458. https://doi.org/10.1016/j.matlet.2020.127458.

(20) Pierini, F.; Lanzi, M.; Nakielski, P.; Pawłowska, S.; Zembrzycki, K.; Kowalewski, T. A. Electrospun Poly(3-Hexylthiophene)/Poly(Ethylene Oxide)/Graphene Oxide Composite Nanofibers: Effects of Graphene Oxide Reduction. *Polym. Adv. Technol.* **2016**, *27* (11), 1465–1475. https://doi.org/10.1002/pat.3816.

(21) Chen, J. Y.; Wu, H. C.; Chiu, Y. C.; Lin, C. J.; Tung, S. H.; Chen, W. C. Electrospun Poly(3-Hexylthiophene) Nanofibers with Highly Extended and Oriented Chains through Secondary Electric Field for High-Performance Field-Effect Transistors. *Adv. Electron. Mater.* **2015**, *1* (1–2), 1–8. https://doi.org/10.1002/aelm.201400028.

(22) Bianco, A.; Bertarelli, C.; Frisk, S.; Rabolt, J. F.; Gallazzi, M. C.; Zerbi, G. Electrospun Polyalkylthiophene/Polyethyleneoxide Fibers: Optical Characterization. *Synth. Met.* **2007**, *157* (6–7), 276–281. https://doi.org/10.1016/j.synthmet.2007.03.006.

(23) Chan, K. H. K.; Yamao, T.; Kotaki, M.; Hotta, S. Unique Structural Features and Electrical Properties of Electrospun Conjugated Polymer Poly(3-Hexylthiophene) (P3HT) Fibers. *Synth. Met.* **2010**, *160* (23–24), 2587–2595. https://doi.org/10.1016/j.synthmet.2010.10.009.

(24) Laforgue, A.; Robitaille, L. Fabrication of Poly-3-Hexylthiophene/Polyethylene Oxide Nanofibers Using Electrospinning. *Synth. Met.* **2008**, *158* (14), 577–584. https://doi.org/10.1016/j.synthmet.2008.04.004.

(25) Hernández-Martínez, D.; Martínez-Alonso, C.; Castillo-Ortega, M. M.; Arenas-Arrocena, M. C.; Nicho, M. E. Preparation and Characterization of Electrospun Fibers Containing Poly(3-Hexylthiophene) and Poly(3-Hexylthiophene)/CdS. *Synth. Met.* **2015**, *209*, 496–501. https://doi.org/10.1016/j.synthmet.2015.09.001.

(26) Hernández-Martínez, D.; Nicho, M. E.; Hu, H.; León-Silva, U.; Arenas-Arrocena, M. C.; García-Escobar, C. H. Electrospinning of P3HT-PEO-CdS Fibers by Solution Method and Their Properties. *Mater. Sci. Semicond. Process.* **2017**, *61* (November 2016), 50–56. https://doi.org/10.1016/j.mssp.2016.12.039.

(27) González, R.; Pinto, N. J. Electrospun Poly(3-Hexylthiophene-2,5-Diyl) Fiber Field Effect Transistor. *Synth. Met.* **2005**, *151* (3), 275–278. https://doi.org/10.1016/j.synthmet.2005.05.007.

(28) Lee, S.; Moon, G. D.; Jeong, U. Continuous Production of Uniform Poly(3-Hexylthiophene) (P3HT) Nanofibers by Electrospinning and Their Electrical Properties. *J. Mater. Chem.* **2009**, *19* (6), 743–748. https://doi.org/10.1039/b814833c.

(29) Liu, H.; Reccius, C. H.; Craighead, H. G. Single Electrospun Regioregular Poly(3-Hexylthiophene) Nanofiber Field-Effect Transistor. *Appl. Phys. Lett.* **2005**, *87* (25), 1–3. https://doi.org/10.1063/1.2149980.

(30) Wu, Q.; Mei, C.; Zhang, X.; Lei, T.; Zhang, Z.; Li, M. Electrospun Poly(Ethylene Oxide) Fibers Reinforced with Poly (Vinylpyrrolidone) Polymer and Cellulose Nanocrystals.

Electrospinning Method Used to Creat. Funct. Nanocomposites Film. **2018**. https://doi.org/10.5772/intechopen.76392.

(31) Himmelberger, S.; Vandewal, K.; Fei, Z.; Heeney, M.; Salleo, A. Role of Molecular Weight Distribution on Charge Transport in Semiconducting Polymers. *Macromolecules* **2014**, *47* (20), 7151–7157. https://doi.org/10.1021/ma501508j.

(32) Kline, R. J.; McGehee, M. D.; Kadnikova, E. N.; Liu, J.; Fréchet, J. M. J.; Toney, M. F. Dependence of Regioregular Poly(3-Hexylthiophene) Film Morphology and Field-Effect Mobility on Molecular Weight. *Macromolecules* **2005**, *38* (8), 3312–3319. https://doi.org/10.1021/ma047415f.

(33) Bielecka, U.; Lutsyk, P.; Janus, K.; Sworakowski, J.; Bartkowiak, W. Effect of Solution Aging on Morphology and Electrical Characteristics of Regioregular P3HT FETs Fabricated by Spin Coating and Spray Coating. *Org. Electron.* **2011**, *12* (11), 1768–1776. https://doi.org/10.1016/j.orgel.2011.06.027.

(34) Kim, D. K.; Hwang, M.; Lagerwall, J. P. F. Liquid Crystal Functionalization of Electrospun Polymer Fibers. *J. Polym. Sci. Part B Polym. Phys.* **2013**, *51* (11), 855–867. https://doi.org/10.1002/polb.23285.

(35) Xiao, G.; Guo, Y.; Lin, Y.; Ma, X. Controlled Evaporative Self-Assembly of Poly (3-Hexylthiophene) Monitored with Confocal Polarized Raman Spectroscopy. *Phys. Chem. Chem. Phys.,* **2012**, 14, 16286–16293. https://doi.org/10.1039/c2cp43435k.

(36) Bastianini, F.; Pérez, G. E.; Hobson, A. R.; Rogers, S. E.; Parnell, A. J.; Grell, M.; Flores, A.; Dunbar, A. D. F. Solar Energy Materials and Solar Cells In − Situ Monitoring Poly (3-

Hexylthiophene) Nanowire Formation and Shape Evolution in Solution via Small Angle Neutron Scattering. *Sol. Energy Mater. Sol. Cells* **2019**, *202* (August), 110128. https://doi.org/10.1016/j.solmat.2019.110128.

(37) Tang, K.; Huang, L.; Lim, J.; Zaveri, T.; Azoulay, J. D.; Guo, S. Chemical Doping of Well-Dispersed P3HT Thin-Film Nanowire Networks. *ACS Appl. Polym. Mater.* **2019**, *1* (11), 2943–2950. https://doi.org/10.1021/acsapm.9b00653.

(38) Aiyar, A. R.; Hong, J. Il; Izumi, J.; Choi, D.; Kleinhenz, N.; Reichmanis, E. Ultrasound-Induced Ordering in Poly(3-Hexylthiophene): Role of Molecular and Process Parameters on Morphology and Charge Transport. *ACS Appl. Mater. Interfaces* **2013**, *5* (7), 2368–2377. https://doi.org/10.1021/am3027822.

(39) Wang, G.; Persson, N.; Chu, P. H.; Kleinhenz, N.; Fu, B.; Chang, M.; Deb, N.; Mao, Y.; Wang, H.; Grover, M. A.; et al. Microfluidic Crystal Engineering of π-Conjugated Polymers. *ACS Nano* **2015**, *9* (8), 8220–8230. https://doi.org/10.1021/acsnano.5b02582.

(40) Niles, E. T.; Roehling, J. D.; Yamagata, H.; Wise, A. J.; Spano, F. C.; Moule, A. J.; Grey, J. K. J-Aggregate Behavior in Poly-3-Hexylthiophene Nanofibers. J. Phys. Chem. Lett. **2012**, 3, 259−263

(41) Lakdusinghe, M.; Abbaszadeh, M.; Mishra, S.; Sengottuvelu, D.; Wijayapala, R.; Zhang, S.; Benasco, A. R.; Gu, X.; Morgan, S. E.; Wipf, D. O.; et al. Nanoscale Self-Assembly of Poly(3-Hexylthiophene) Assisted by a Low-Molecular-Weight Gelator toward Large-Scale Fabrication of Electrically Conductive Networks. *ACS Appl. Nano Mater.* **2021**, 4, 8, 8003–8014, https://doi.org/10.1021/acsanm.1c01294.

(42) Shenoy, S. L.; Bates, W. D.; Frisch, H. L.; Wnek, G. E. Role of Chain Entanglements on Fiber Formation during Electrospinning of Polymer Solutions: Good Solvent, Non-Specific Polymer-Polymer Interaction Limit. *Polymer (Guildf).* **2005**, *46* (10), 3372–3384. https://doi.org/10.1016/j.polymer.2005.03.011.

(43) Chronakis, I. S.; Grapenson, S.; Jakob, A. Conductive Polypyrrole Nanofibers via Electrospinning: Electrical and Morphological Properties. *Polymer (Guildf).* **2006**, *47* (5), 1597–1603. https://doi.org/10.1016/j.polymer.2006.01.032.

(44) A. Koski, K. Yim, S. Shivkumar, Effect of molecular weight on fibrous PVA produced by electrospinning, *Materials Letters*. 2004, 58, 3–4, 493-497. https://doi.org/10.1016/S0167-577X(03)00532-9.

(45) Akduman, Ç.; Kumabasar, E. P. A.; Çay, A. Effect of molecular weight on the morphology of electrospun poly (vinyl alcohol) nanofibers. *XIIIth International Izmir Textile and Apparel Symposium*. **2014**, 127–134.

(46) Filip, P.; Peer, P. Characterization of Poly(Ethylene Oxide) Nanofibers-Mutual Relations between Mean Diameter of Electrospun Nanofibers and Solution Characteristics. *Processes* **2019**, *7* (12). https://doi.org/10.3390/PR7120948.

(47) Yeong, B.; Park, D.; Lee, H. S.; Choi, Y. J.; Kwak, D.; Cho, H.; Lee, S.; Cho, K. Solubility-Induced Ordered Polythiophene Precursors for High-Performance Organic Thin-Film Transistors. *Adv. Funct. Mater.* **2009**, 19, 1200–1206. https://doi.org/10.1002/adfm.200801763.

(48) Wolf, C. M.; Guio, L.; Scheiwiller, S. C.; Hara, R. P. O.; Luscombe, C. K.; Pozzo, L. D. Blend Morphology in Polythiophene−Polystyrene Composites from Neutron and X-Ray

Scattering. *Macromolecules* **2021,** 54, 2960−2978. https://doi.org/10.1021/acs.macromol.0c02512.

(49) Chen, C. Y.; Chan, S. H.; Li, J. Y.; Wu, K. H.; Chen, H. L.; Chen, J. H.; Huang, W. Y.; Chen, S. A. Formation and Thermally-Induced Disruption of Nanowhiskers in Poly(3-Hexylthiophene)/Xylene Gel Studied by Small-Angle X-Ray Scattering. *Macromolecules* **2010**, *43* (17), 7305–7311. https://doi.org/10.1021/ma1008034.

(50) Kajiya, D.; Saitow, K. I. Ultrapure Films of Polythiophene Derivatives Are Born on a Substrate by Liquid Flow. *ACS Appl. Energy Mater.* **2018**, *1* (12), 6881–6889. https://doi.org/10.1021/acsaem.8b01260.

(51) Spano, F. C.; Silva, C. H- and J-Aggregate Behavior in Polymeric Semiconductors. *Annu. Rev. Phys. Chem.* **2014**, *65* (January), 477–500. https://doi.org/10.1146/annurev-physchem-040513-103639.

(52) Spano, F. C. The Spectral Signatures of Frenkel Polarons in H- And J-Aggregates. *Acc. Chem. Res.* **2010**, *43* (3), 429–439. https://doi.org/10.1021/ar900233v.

(53) Martin, T. P.; Wise, A. J.; Busby, E.; Gao, J.; Roehling, J. D.; Ford, M. J.; Larsen, D. S.; Moulé, A. J.; Grey, J. K. Packing Dependent Electronic Coupling in Single Poly(3-Hexylthiophene) H- and J-Aggregate Nanofibers. *J. Phys. Chem. B* **2013**, *117* (16), 4478–4487. https://doi.org/10.1021/jp308586k.

(54) Kim, T.; Im, J. H.; Choi, H. S.; Yang, S. J.; Kim, S. W.; Park, C. R. Preparation and Photoluminescence (PL) Performance of a Nanoweb of P3HT Nanofibers with Diameters below 100 Nm. *J. Mater. Chem.* **2011**, *21* (37), 14231–14239. https://doi.org/10.1039/c1jm10396b.

(55) Panzer F, Bässler H, Ko, A. Temperature Induced Order − Disorder Transition in Solutions of Conjugated Polymers Probed by Optical Spectroscopy. *The journal of physical chemistry letters.* **2017**. 8(1):114-25. https://doi.org/10.1021/acs.jpclett.6b01641.

(56) Chen, T.; Wu, X.; Rieke, R. D. Poly(3-Alkylthiophenes) Mediated by Rieke Zinc: Their Characterization. *J. Am. Chem. Soc.* **1995**, 117, 1, 233–244.

(57) Hernández-Martínez, D.; Nicho, M. E.; Alvarado-Tenorio, G.; García-Carvajal, S.; Castillo-Ortega, M. M.; Vásquez-López, C. Elaboration and Characterization of P3HT–PEO–SWCNT Fibers by Electrospinning Technique. *SN Appl. Sci.* **2020**, *2* (3). https://doi.org/10.1007/s42452-020-2278-2.

(58) Hashemnejad, S. M.; Kundu, S. Rheological Properties and Failure of Alginate Hydrogels with Ionic and Covalent Crosslinks. *Soft Matter* **2019**, *15* (39), 7852–7862. https://doi.org/10.1039/c9sm01039d.

(59) Mishra, S.; Badani Prado, R. M.; Kundu, S. Concentration-Dependent Mechanical Behavior of Physically Assembled Triblock Copolymer Gels. *ACS Appl. Polym. Mater.* **2020**, *2* (12), 5388–5397. https://doi.org/10.1021/acsapm.0c00583.

(60) Prado, R. M. B.; Mishra, S.; Ahmad, H.; Burghardt, W. R.; Kundu, S. Capturing the Transient Microstructure of a Physically Assembled Gel Subjected to Temperature and Large Deformation. *Macromolecules* **2021**, *54* (19), 8946–8959. https://doi.org/10.1021/acs.macromol.1c00895.

(61) Hashemnejad, S. M.; Kundu, S. Probing Gelation and Rheological Behavior of a Self-Assembled Molecular Gel. *Langmuir* **2017**, *33* (31), 7769–7779. https://doi.org/10.1021/acs.langmuir.7b01531.

(62) Maria, R.; Prado, B.; Mishra, S.; Ahmed, H.; Burghardt, R. Soft Matter Endblock-Associated Triblock Gels of Different Block Lengths in a Midblock Selective Solvent †. *Soft Matter.* **2022**, 18, 7020-7034. https://doi.org/10.1039/d2sm00567k.

(63) Newbloom, G. M.; De La Iglesia, P.; Pozzo, L. D. Controlled Gelation of Poly(3-Alkylthiophene)s in bulk and in Thin-Films Using Low Volatility Solvent/Poor-Solvent Mixtures. *Soft Matter* **2014**, *10* (44), 8945–8954. https://doi.org/10.1039/c4sm00960f.

(64) Newbloom, G. M.; Weigandt, K. M.; Pozzo, D. C. Electrical, Mechanical, and Structural Characterization of Self-Assembly in Poly(3-Hexylthiophene) Organogel Networks. *Macromolecules* **2012**, *45* (8), 3452–3462. https://doi.org/10.1021/ma202564k.

(65) Newbloom, G. M.; Kim, F. S.; Jenekhe, S. A.; Pozzo, D. C. Mesoscale Morphology and Charge Transport in Colloidal Networks of Poly(3-Hexylthiophene). *Macromolecules* **2011**, *44* (10), 3801–3809. https://doi.org/10.1021/ma2000515.

(66) Samitsu, S.; Shimomura, T.; Ito, K. Nanofiber Preparation by Whisker Method Using Solvent-Soluble Conducting Polymers. *Thin Solid Films.* **2008**, *516*, 2478–2486. https://doi.org/10.1016/j.tsf.2007.04.058.

(67) Merchiers, J.; Martínez Narváez, C. D. V.; Slykas, C.; Reddy, N. K.; Sharma, V. Evaporation and Rheology Chart the Processability Map for Centrifugal Force Spinning. *Macromolecules* **2021**, *54* (23), 11061–11073. https://doi.org/10.1021/acs.macromol.1c01799.

(68) Xu, X.; Jiang, L.; Zhou, Z.; Wu, X.; Wang, Y. Preparation and Properties of Electrospun Soy Protein Isolate/Polyethylene Oxide Nanofiber Membranes. *ACS Appl. Mater. Interfaces* **2012**, *4* (8), 4331–4337. https://doi.org/10.1021/am300991e.

(69) Pierini, F.; Lanzi, M.; Nakielski, P.; Pawlowska, S.; Urbanek, O.; Zembrzycki, K.; Kowalewski, T. A. Single-Material Organic Solar Cells Based on Electrospun Fullerene-Grafted Polythiophene Nanofibers. *Macromolecules* **2017**, *50* (13), 4972–4981. https://doi.org/10.1021/acs.macromol.7b00857.

(70) Na, J. Y.; Kang, B.; Park, Y. D. Influence of Molecular Weight on the Solidification of a Semiconducting Polymer during Time-Controlled Spin-Coating. *J. Phys. Chem. C*. **2019**. 123, 17102−17111, https://doi.org/10.1021/acs.jpcc.9b03203.

(71) Deitzel, J. M.; Kleinmeyer, J.; Harris, D.; Beck Tan, N. C. The Effect of Processing Variables on the Morphology of Electrospun. *Polymer (Guildf).* **2001**, *42*, 261–272.

(72) Perez, L. A.; Zalar, P.; Ying, L.; Schmidt, K.; Toney, M. F.; Nguyen, T. Q.; Bazan, G. C.; Kramer, E. J. Effect of Backbone Regioregularity on the Structure and Orientation of a Donor-Acceptor Semiconducting Copolymer. *Macromolecules* **2014**, *47* (4), 1403–1410. https://doi.org/10.1021/ma4019679.

(73) Lee, J. Y.; Kang, T. H.; Choi, J. H.; Choi, I. S.; Yu, W. R. Improved Electrical Conductivity of Poly(Ethylene Oxide) Nanofibers Using Multi-Walled Carbon Nanotubes. *AIP Adv.* **2018**, *8* (3). https://doi.org/10.1063/1.5026509.

(74) Jacobs, I. E.; Aasen, E. W.; Oliveira, J. L.; Fonseca, T. N.; Roehling, J. D.; Li, J.; Zhang, G.; Augustine, M. P.; Mascal, M.; Moulé, A. J. Comparison of Solution-Mixed and Sequentially

Processed P3HT:F4TCNQ Films: Effect of Doping-Induced Aggregation on Film Morphology. *J. Mater. Chem. C* **2016**, *4* (16), 3454–3466. https://doi.org/10.1039/c5tc04207k.

(75) Malik, S.; Jana, T.; Nandi, A. K. Thermoreversible Gelation of Regioregular Poly(3-Hexylthiophene) in Xylene. *Macromolecules* **2001**, *34* (2), 275–282. https://doi.org/10.1021/ma000977o.

(76) Lim, E.; Peterson, K. A.; Su, G. M.; Chabinyc, M. L. Thermoelectric Properties of Poly(3-Hexylthiophene) (P3HT) Doped with 2,3,5,6-Tetrafluoro-7,7,8,8-Tetracyanoquinodimethane (F4TCNQ) by Vapor-Phase Infiltration. *Chem. Mater.* **2018**, *30* (3), 998–1010. https://doi.org/10.1021/acs.chemmater.7b04849.

For Table of Contents use only

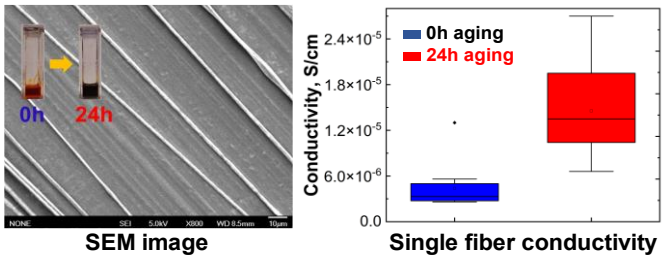

Effects of Poly(3-hexylthiophene) Molecular Weight and the Aging of Spinning Solution on the Electrospun Fiber Properties

Humayun Ahmad,[†] *Song Zhang,*[‡] *Chih-Ting Liu,*[‡] *Guorong Ma,*[‡], *Jason D. Azoulay,*[‡] *Xiaodan Gu,*[‡] *Mahesh K Gangishetty,*[¦] *Santanu Kundu*[†]*

[†]Dave C. Swalm School of Chemical Engineering, Mississippi State University, MS State, MS 39762, United States

[‡] School of Polymer Science and Engineering, University of Southern Mississippi, Hattiesburg, MS 39406, USA

[¦]Department of Chemistry & Department of Physics and Astronomy, Mississippi State University, MS State, MS 39762, United States